

Operability of Thermomechanical Titanium Nickelide Actuators

M. Yu. Kollerov^a, D. E. Gusev^{a, *}, A. A. Sharonov^a, and A. O. Snegirev^a

^a Moscow Aviation Institute (National Research University), Moscow, 125993 Russia

*e-mail: gusev-home@mail.ru

Received January 26, 2022; revised February 2, 2022; accepted February 6, 2022

Abstract—The operability of shape memory spring actuators made of titanium nickelide under constant and variable counteraction to shape recovery is investigated. Methods for calculating the maximum specific energy of the actuators using the properties of the material are proposed. These properties are shown to be the critical strains and stresses (in martensitic and austenitic states) corresponding to the beginning of slip processes and depending on the ratio of the test temperature to the shape recovery temperatures.

Keywords: actuator, spring, specific energy, shape memory effect, titanium nickelide, critical stresses and strains

DOI: 10.1134/S0036029522100317

1. INTRODUCTION

Actuators are the devices that convert a control signal into useful work with an actuator; in most cases, they are electromechanical and have large overall dimensions [1]. The actuators can use functional materials with special properties, such as the piezoelectric effect, magnetostriction, and the shape memory effect [2, 3]. Piezo- and magnetostriction actuators are characterized by a high response frequency (up to 10000 Hz) but have a low specific power [4]. Actuators made of shape memory effect (SME) alloys are characterized by a low response frequency (lower than 1 Hz) but can perform three orders of magnitude higher specific work, and a combination of a thermosensitive element and an actuating mechanism in such actuators makes it possible to minimize their dimensions and weight [4, 5].

Actuators made of titanium nickelide-based alloys are most widely used among the developed and tested SME actuators [5]. They are used in automatic temperature controllers of air conditioning and water supply systems, car thermostats, press drives, mechanisms for changing the wing profile of aircraft, and heat engines [5–8]. The basic principles of designing such actuators have been studied in sufficient detail [2, 3, 5, 9–14]. It is believed that, when actuators in the form of torsion tubes [15] or spiral springs [16, 17] are used, it is possible to achieve a combination of the highest functional characteristics with the simplicity and compactness of an actuator design.

The operability of SME actuators is largely determined by a set of the temperature, strain, force, and energy characteristics of such materials. However, the scientifically based principles to improve the effi-

ciency of SME actuators have not yet been fully determined. As a rule, they consist in choosing a material with the desired SME temperature range [18]. The authors of [9, 19, 20] demonstrated a high sensitivity of both temperature and strain and force characteristics of SME to the structure of titanium nickelide-based alloys, which depends on both the chemical composition of the alloy and on the technology of producing semifinished and end products.

The purpose of this work is to find the relationship between the performance characteristics of spring thermomechanical actuators (reversible strain, developed forces, specific energy) and their geometric parameters and the properties of an SME material. The critical stresses and strains, at which slip processes begin to develop in an alloy and lead to incomplete shape recovery (if they are exceeded, the operability of the actuators should decrease), were chosen as such characteristics [21, 22]. This fact is a limitation of the operating conditions for multiple operating actuators.

2. EXPERIMENTAL

A wire 1.3 mm in diameter made of a Ti–55.8Ni alloy (wt %) was used as an object of research. The alloy is an aging alloy with the possibility of precipitation of nickel-rich Ti_3Ni_4 and Ti_2Ni_3 intermetallic particles at temperatures of 400–500°C [23], which allows us to vary the temperature of the end of the reverse martensitic transformation (A_f) over a fairly wide range, from –30 to 50°C.

Straight pieces of wire were subjected to torsion tests in an inverse torsion pendulum at temperatures from 20 to 100°C. Using experimental results, we plotted stress–strain curves in the conventional tangential

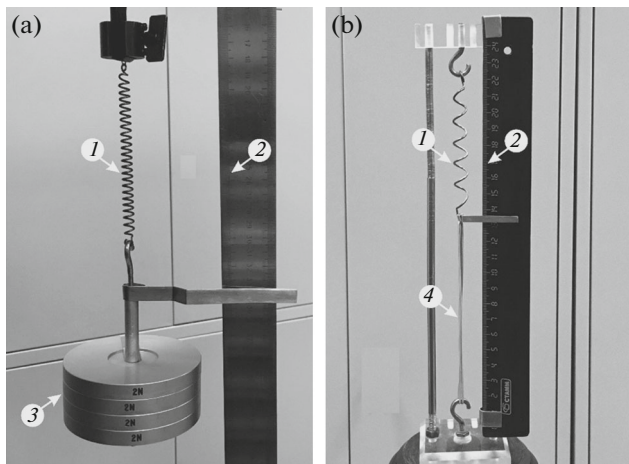


Fig. 1. Devices for testing SME springs under (a) constant and (b) variable shape recovery counteraction: (1) spring to be tested, (2) spring elongation scale, (3) loads, and (4) rubber bundles.

stress τ –shear strain γ coordinates and the temperature dependences of the following mechanical characteristics: conventional yield strength $\tau_{0.3}$ (not related to slip, but is the phase yield strength) and critical stress $\tau_{cr}^{0.3}$ and strain $\gamma_{cr}^{0.3}$ at which an unrecoverable strain of 0.3% accumulates in the material [21].

Conventional tangential stresses τ and shear strains γ appearing on the outer surface of the wire samples during torsion were estimated according to GOST 3565–80 by the formulas

$$\tau = \frac{16M_{tor}}{\pi d^3}, \quad (1)$$

$$\gamma = \frac{\varphi d}{2l}, \quad (2)$$

where M_{tor} is the torque, φ is the angle of torsion, d is the diameter of the wire sample, and l is the gage length of the sample (70 mm).

The thermomechanical behavior of the springs acting as the actuator of an actuator mock-up was also investigated. The springs were formed by winding a wire on a cylindrical tooling at a temperature of $21 \pm 1^\circ\text{C}$ and subsequent thermal fixation in a constrained state at 550°C for 1 h. Hooks were formed at the ends of the springs upon heating by a gas burner to 550 – 600°C .

The wire samples and springs were vacuum annealed at 700°C and then subjected to aging at 470°C for 1 h. As a result of this treatment, the temperatures of the onset (A_s^r) and end (A_s^f) of the shape recovery of the wire samples and springs deformed by bending or tension by 2–2.5% (according to ASTM F2082/F2082M [24]), respectively, and heated in a free-standing state in a water thermostat were $A_s^r =$

$38 \pm 3^\circ\text{C}$ and $A_s^f = 45 \pm 2^\circ\text{C}$. According to X-ray diffraction studies, the alloy structure at 20°C was represented by the B2 phase with a small number of B19' martensite plates and Ti_2Ni and Ti_3Ni_4 intermetallic particles. Finishing treatment included the removal of oxidized layers and polishing of the surface using ceramic and polymer materials.

The actuator mock-ups were tested according to the following two schemes: at constant counteraction to shape recovery, when a load of various weights was attached to a vertically suspended spring (Fig. 1a), and at variable counteraction, for which various numbers of rubber bundles used as an elastic counterbody were attached to the spring; then, a spring–counterbody pair was attached inside a rigid rectangular frame (Fig. 1b). Both the number of bundles with known stiffness and the initial (before connection) distance between the spring and the bundles were varied. The springs were heated by a hot air flow. The temperature was controlled with a chromel–copel thermocouple.

During heating and cooling, the change in the spring length ΔL was detected to calculate the strain of the material at temperatures of 20 (γ_M) and 100°C (γ_A). In addition, we determined the unrecoverable strain γ_{ur} after heating to 100°C in a free-standing state and the reversible strain γ_{rev} as the difference between γ_M and γ_A . Testing of the springs was stopped after the appearance of an unrecoverable strain in them.

Conventional tangential stresses τ and shear strains γ that appear on the outer surface of the springs during tests were estimated using the formulas [5, 25]

$$\tau = \frac{8PD}{\pi d^3} \left(\frac{4C-1}{4C-4} + \frac{0.615}{C} \right), \quad (3)$$

$$\gamma = \frac{\Delta L d}{\pi n D^2}, \quad (4)$$

where P is the external tensile load, D is the average spring coil diameter, d is the diameter of the wire from which the spring is made, $C = D/d$ is the spring index, ΔL is the elongation of the spring, and n is the number of working spring coils.

The specific energy of the actuator (a) was calculated as the ratio of the work performed by it (A) to the spring volume (V), $a = A/V$, using the load displacement or the elongation of the rubber bundles during heating from 20 to 100°C .

3. RESULTS

3.1. Thermomechanical Behavior of Ti–55.8Ni Alloy

The thermomechanical behavior of a Ti–55.8 Ni alloy should be considered at various temperatures to correctly analyze the operability of SME actuators (Fig. 2). At 20°C , the material is characterized by a low yield strength ($\tau_{0.3} \approx 80$ MPa) corresponding to the

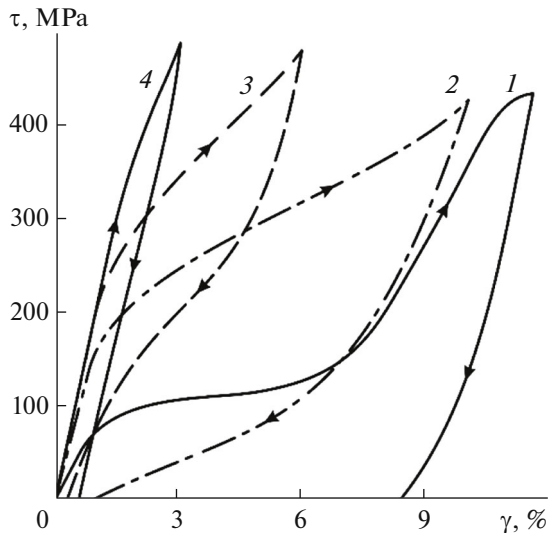


Fig. 2. Stress–strain curves for torsion tests of Ti–55.8Ni alloy wire samples at a temperature of (1) 20, (2) 60, (3) 80, and (4) 100°C.

stresses of formation or twinning/detwinning of martensite followed by an extended section with insignificant strain resistance in the τ – γ diagram. At strain $\gamma > 6$ –7%, stress τ grows intensely. If the loading process stops on the flat section of the stress–strain diagram, a slight strain of 0.5–1.5% is eliminated after unloading, and the residual strain disappears completely upon heating above the temperature of the end of the reverse martensitic transformation (A_f). When the total strain of the material (10%) is reached, a strain not recovered upon heating ($\gamma_{ur} = 0.2$ –0.3%) appears; it increases intensely with further loading.

Thus, the total strain ($\gamma = 10\%$) and the corresponding stress $\tau = 350$ MPa are critical for the alloy in the martensitic state. It should be noted that $\tau_{cr}^{0.3} = 350$ MPa is lower than the stresses at which the “second yield strength” of the alloy, namely, intense slip in martensite, is observed.

When the test temperature increases, the martensitic shear stresses increase; at temperatures above the temperature of the end of the reverse martensitic transformation A_f , the martensitic strain accumulated upon loading is eliminated upon unloading due to the superelasticity of the material (see Fig. 2; curves 2, 3). When the critical stresses and strains are reached in the samples exhibiting superelastic behavior, unrecoverable strain caused by slip in the material also accumulates. For the alloy in the austenitic state, we detected $\tau_{cr}^{0.3} = 430$ MPa and $\gamma_{cr}^{0.3} = 2.5\%$ at $t = 100^\circ\text{C}$.

The critical stresses and strains of the material depend on the ratio of the test temperature t and to the temperatures of the reverse martensitic transformation A_s and A_f (Fig. 3). At $t > A_f$, the critical strain decreases

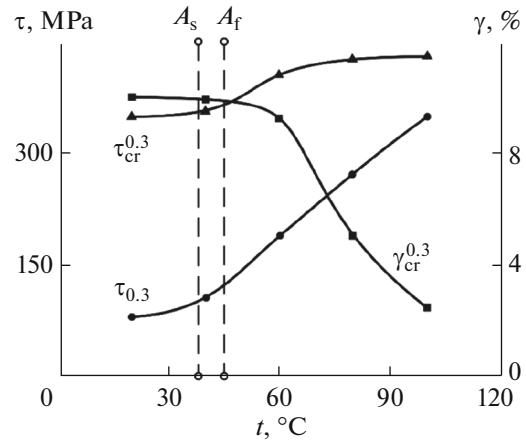


Fig. 3. Temperature dependences of the yield strength ($\tau_{0.3}$), critical stress ($\tau_{cr}^{0.3}$), and critical strain ($\gamma_{cr}^{0.3}$) of Ti–55.8Ni alloy.

significantly. When the temperature increases, $\tau_{cr}^{0.3}$ approaches the critical value and the mechanical behavior of the alloy becomes similar to the behavior of structural materials because of the gradual loss of superelastic properties (see Fig. 2, curve 4).

The found features of the thermomechanical behavior of the Ti–55.8Ni alloy were taken into account to conduct experiments on thermal cycling of the springs under constant and variable counteraction.

3.2. Operability of Springs under Constant Shape Recovery Counteraction

In the experiments, springs with $d = 1.3$ mm, $D = 7.2$ mm, and $n = 22$ were used. A load was suspended from a spring mounted on a bracket, and its weight was increased after each heating (up to 100°C) and cooling (up to 20°C) cycle.

When the constant counteraction stress τ increases, strains γ_M and γ_A change (Fig. 4) similarly to the change established during torsion tests of the straight wire alloy samples (at the corresponding temperatures), and the reversible strain increases until slip processes begin to develop intensely in the spring material. At higher τ stresses exceeding the critical stress of the material in the martensitic state ($\tau_{cr}^{0.3})_M$, unrecoverable strain γ_{ur} appears and the growth of reversible strain γ_{rev} slows down. γ_{rev} reaches a maximum at the stresses τ corresponding to the critical stresses in the austenitic state ($\tau_{cr}^{0.3})_A$. A further increase in τ leads to a decrease in γ_{rev} and an intense accumulation of γ_{ur} . The higher critical strains ($(\gamma_{cr}^{0.3})_M = 10.5\%$, $(\gamma_{cr}^{0.3})_A = 3\%$) than those of the torsion-tested wire samples and the lower critical stresses

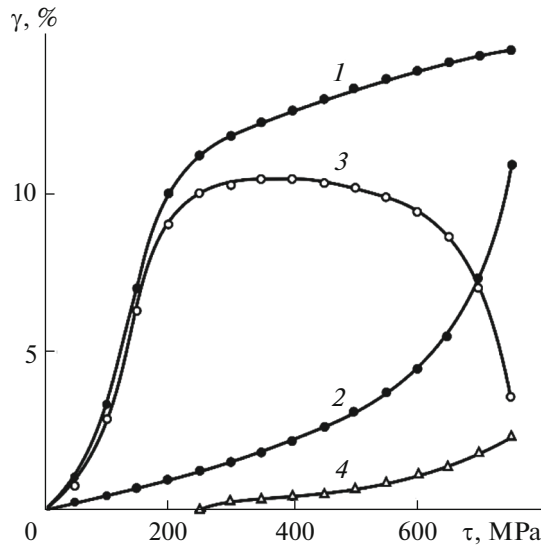


Fig. 4. Influence of the level of constant stresses (τ) that counteract shape recovery on strain (1) γ_M , (2) γ_A , (3) γ_{rev} , and (4) γ_{ur} upon heating from 20 to 100°C.

$((\tau_{cr}^{0.3})_M = 300 \text{ MPa}, (\tau_{cr}^{0.3})_A = 400 \text{ MPa})$ detected during tests of the springs are caused by the additional strain of the spring hooks, which was not taken into account on calculating these quantities.

As the test results showed, the maximum specific energy of the spring is $a_{max} = 12.0 \text{ MJ/m}^3$ under the conditions favorable for repeated operation of the actuator, when the condition $\gamma_{ur} \leq 0.3\%$ is met during thermal cycling. For single actuators, it is advisable to determine a_{max} at the maximum value γ_{rev} , when the

unrecovered strain is $\gamma_{ur} > 0.3\%$. In this case, the specific energy of the spring material reaches 16.4 MJ/m^3 .

3.3 Operability of Springs under Variable Shape Recovery Counteraction

To test the actuator elements under variable counteraction conditions, we used springs with $d = 1.3 \text{ mm}$, $D = 9.2 \text{ mm}$, and $n = 5$, which were connected in a tensioned state with rubber bundles inside a rigid metal frame. In this case, an important characteristic of the actuator is the initial distance ΔL_{ini} between an SME spring and an elastic counterbody, which are in an undeformed state before being connected to form an actuator. Using bundles of different lengths, we changed ΔL_{ini} : it was 87 or 135 mm. The rubber bundles were previously subjected to tensile tests to determine their stiffness. As a result, we were able to determine the forces P that appear during by the interaction of the spring and the counteracting elements at the boundary thermal cycling temperatures (20 and 100°C) using the elongation of the bundles.

The tests (Fig. 5) showed that, when the counterbody counteraction stiffness is varied (by changing the number of bundles), force P and spring elongation ΔL at temperatures of 20 and 100°C are described by curves, which are similar to the τ – γ dependences obtained during torsion of the wire samples (see Fig. 2) and are independent of initial distance ΔL_{ini} . The reversible elongation of the spring increases with the counterbody stiffness K_s and distance ΔL_{ini} . The maximum reversible elongation detected in experiments at a counterbody counteraction stiffness of 0.48 N/mm and $\Delta L_{ini} = 135 \text{ mm}$ was 65 mm, which

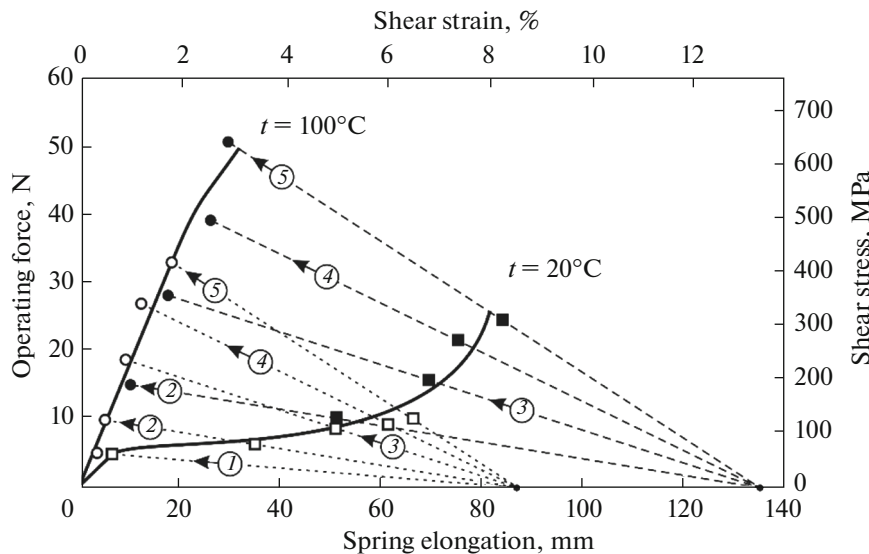


Fig. 5. Influence of the counterbody counteraction stiffness on the operating forces and elongation of a Ti–55.8Ni alloy spring at (squares) 20 and (circles) 100°C at an initial counterbody–spring distance $\Delta L_{ini} =$ (open symbols) 87 and (solid symbols) 135 mm. The numerals in circles indicate the counteraction stiffness: (1) 0.06, (2) 0.12, (3) 0.24, (4) 0.36, and (5) 0.48 N/mm.

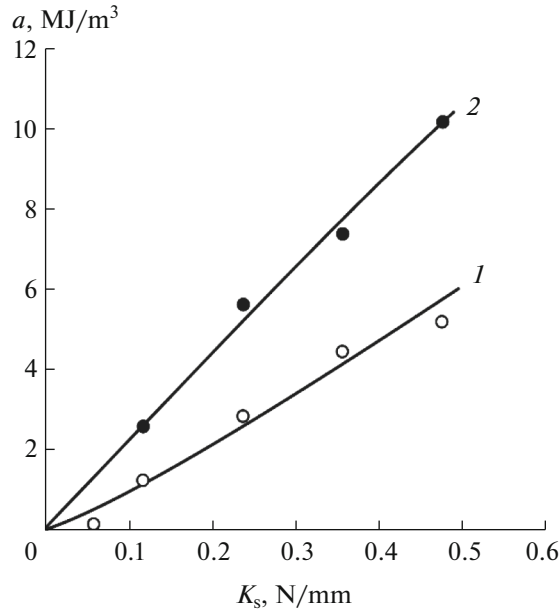


Fig. 6. Influence of counterbody counteraction stiffness K_s and initial distance ΔL_{ini} on the specific work a performed by the spring material of a Ti-55.8Ni alloy actuator under variable counteraction: $\Delta L_{ini} = (1)$ 87 and (2) 135 mm.

corresponds to $\gamma_{rev} = 6.4\%$. This is smaller than this quantity (10.5%) obtained in the constant counteraction experiments.

The specific energy performed by the spring depends on the counterbody stiffness K_s and the initial distance ΔL_{ini} (Fig. 6). The larger the value of K_s , the higher the developed forces. When ΔL_{ini} increases, the reversible elongation of the spring induced by temperature changes also increases. Both factors increase the work performed by the spring. The maximum specific energy achieved in experiments was 10.1 MJ/m^3 (see Fig. 6).

It should be noted that, as stresses and strains increase, the unrecoverable strain would accumulate in the spring material when their critical values are reached, which should lead to a gradual decrease in the efficiency of the actuator. In this case, the specific energy should reach its maximum and then inevitably decrease. This behavior was not observed in our studies, which is likely to be related to the insufficiently high stiffness of the rubber bundles (0.06–0.48 N/mm) and to ΔL_{ini} (87 and 135 mm).

4. DISCUSSION

To find the relationship between the performance characteristics of the actuator and the properties of the SME material, we consider the scheme of its operation under constant counteraction conditions (Fig. 7a). We set an arbitrary stress level in the material τ caused by weight P suspended from the spring. At a low tempera-

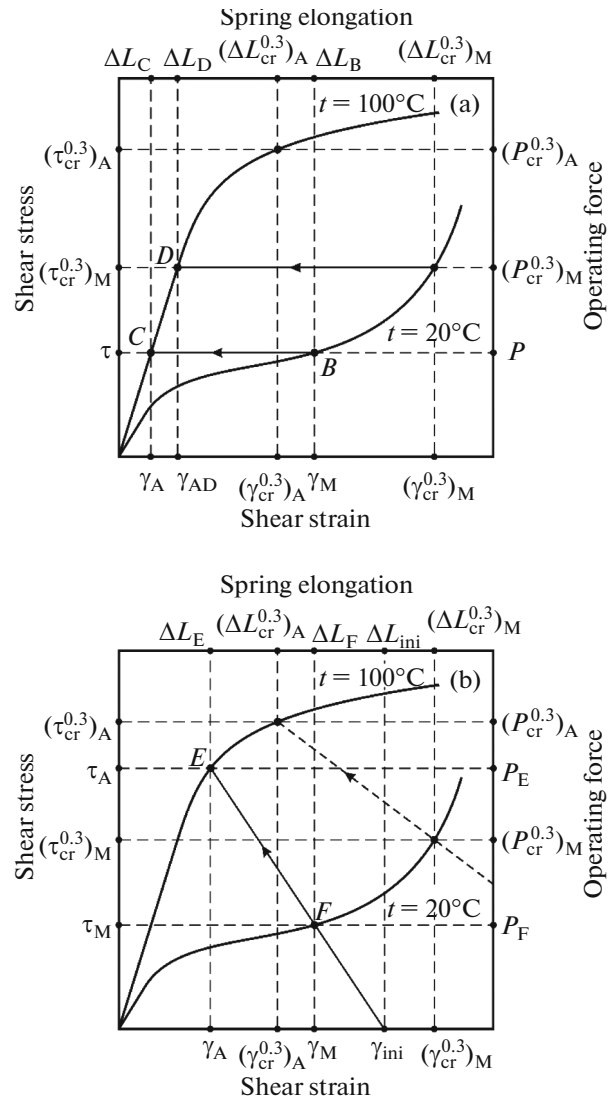


Fig. 7. Stress τ –strain γ curves of titanium nickelide springs at a temperature of 20 and 100°C and the scheme of spring actuator operation under (a) constant and (b) variable counteraction.

ture, the spring material is in the martensitic state and is deformed to point B . The equilibrium of the spring at a high temperature (austenitic state of the alloy) corresponds to point C . The SME-induced specific energy of the spring is

$$a = \frac{P(\Delta L_B - \Delta L_C)}{V} = \frac{\tau}{2k} (\gamma_M - \gamma_A), \quad (5)$$

where $k = \frac{4C - 1}{4C - 4} + \frac{0.615}{C}$ is the correction coefficient (see Eq. (3)) and γ_M and γ_A are the strain of the material under the action of stress τ in the martensitic (point B) and austenitic (point C) states, respectively.

To calculate the maximum possible work performed by the spring in the martensitic state and cor-

responding to the maximum permissible strain $((\gamma_{cr}^{0.3})_M)$ and stress $((\tau_{cr}^{0.3})_M)$, we use the expression

$$\begin{aligned} a_{\max} &= \frac{(\tau_{cr}^{0.3})_M}{2k} [(\gamma_{cr}^{0.3})_M - \gamma_{AD}] \\ &= \frac{(\tau_{cr}^{0.3})_M}{2k} \left[(\gamma_{cr}^{0.3})_M - \frac{(\tau_{cr}^{0.3})_M}{G_A} \right], \end{aligned} \quad (6)$$

where γ_{AD} is the strain of the spring upon heating to the austenitic state (at point *D*) and G_A is the shear modulus of the alloy in the austenitic state.

It should be noted that the operability of multiple-acting actuators should be limited to critical stress $(\tau_{cr}^{0.3})_M$, since an unrecoverable strain begins to accumulate in the material when it is exceeded, which would lead to the loss of the initial shape of the spring element. For single-acting actuators, this limitation is not so fundamental. For them, a higher stress level can be applied, which provides an increase in the specific shape recovery energy due to incomplete return to the initial shape.

Since $G_A \approx 30$ GPa for the alloy under study and $k \approx 1.2$ for the springs, the maximum specific energy at constant shape recovery counteraction calculated by Eq. (6) can reach 12.8 MJ/m³, which is close to the value experimentally obtained in the work (12.0 MJ/m³). The slight discrepancy can be due to the fact that the conventional stresses used in the calculation are slightly higher than the true stresses acting in the outer layers of the wire. It should also be noted that the theoretical calculation of the maximum energy of the spring does not take into account the contribution of its hooks to the total strain.

The situation for variable counteraction actuators (connection of an SME spring with a steel counter spring or rubber bundles) is more complicated, since it is necessary to take into account the stiffness of the counteracting counterbody K_s and the preliminary distance ΔL_{ini} between the SME spring and the counterbody before their connection. For this purpose, it is necessary to lay off initial distance ΔL_{ini} in the stress–strain diagram to the right (Fig. 7b) and to plot a straight line from this distance toward its decrease at the slope corresponding to the stiffness of the spring K_s . The system of an SME spring and a counter spring is in equilibrium at point *F* at a low temperature and at point *E* at a high temperature. In this case, it is advisable to replace parameters K_s and ΔL_{ini} with equivalent characteristics describing the corresponding stress–strain state of the SME spring. In this case, the stiffness of the counter spring, which can be determined as $K_s = (P_A - P_M) / (\Delta L_M - \Delta L_A)$, is characterized by the conventional modulus of counteraction $G_s = (\tau_A - \tau_M) / (\gamma_M - \gamma_A)$ and the initial distance between the springs ΔL_{ini} is characterized by initial strain γ_{ini} .

The specific work performed by the spring is

$$\begin{aligned} a &= \frac{(P_F + P_E)(\Delta L_F - \Delta L_E)}{2V} \\ &= \frac{(\tau_M + \tau_A)}{4k} (\gamma_M - \gamma_A). \end{aligned} \quad (7)$$

The maximum specific energy of the spring can be reached when the counteracting spring provides the stresses closest to the critical ones at low and high temperatures. Such conditions are met at

$$G_s = \frac{(\tau_{cr}^{0.3})_A - (\tau_{cr}^{0.3})_M}{(\gamma_{cr}^{0.3})_M - (\gamma_{cr}^{0.3})_A}, \quad (8)$$

$$\gamma_{ini} = (\gamma_{cr}^{0.3})_A + \frac{(\tau_{cr}^{0.3})_A}{G_s}. \quad (9)$$

Then, we have

$$a_{\max} = \frac{(\tau_{cr}^{0.3})_A + (\tau_{cr}^{0.3})_M}{4k} [(\gamma_{cr}^{0.3})_M - (\gamma_{cr}^{0.3})_A]. \quad (10)$$

For springs made of a Ti–55.8Ni alloy, the maximum possible specific energy under variable shape recovery counteraction, which is calculated by Eq. (10), can reach 11.7 MJ/m³, which is somewhat lower than that under constant counteraction (12.8 MJ/m³). This result also agrees well with the experiment, in which the condition of achieving a_{\max} under variable counteraction was not met and the detected maximum specific energy was 10.1 MJ/m³.

5. CONCLUSIONS

An analysis of the thermomechanical behavior of SME spring actuators showed that their operability is determined by both geometric design parameters (spring coil diameter *D*, wire diameter *d*, spring index $C = D/d$, the number of working turns of a spring *n*) and the critical stresses and strains of the material in martensitic and austenitic states. This fact should be taken into account for designing actuators. It is especially important that, according to [21, 22], these critical characteristics of titanium nickelide-based alloys depend on both the chemical composition of an alloy and its structure, which forms during the production of semi-finished products and their treatment.

The formulas proposed in this work are intended to estimate the maximum possible specific shape recovery energy of SME actuators under constant and variable counteraction conditions with allowance for the properties of the material. These formulas allow us to choose the design of spring actuators and the most efficient technology for their treatment, which ensures the optimum structure of the material with the highest critical stresses and strains. The results of testing springs made of a titanium nickelide-based alloy confirmed the possibility of using these formulas for calculating the specific energy of actuators.

FUNDING

This work was carried out within the framework of the basic part of state task no. FSFF-2020-0017 for universities using the equipment of the core facility “Aerospace Materials and Technologies” of the Moscow Aviation Institute.

CONFLICT OF INTEREST

The authors declare that they have no conflicts of interest.

REFERENCES

1. C.W. De Silva, *Sensors and Actuators: Engineering System Instrumentation* (Taylor & Francis Group, 2016).
2. M. Kohl, *Shape Memory Microactuators* (Springer, Berlin, 2004).
3. M. Mertmaun and G. Vergani, “Design and application of shape memory actuators,” *Eur. Phys. J. Special Topics* **158** (1), 221–230 (2008).
4. A. Nespoli, E. Biffi, R. Casati, F. Passaretti, A. Tuissi, and E. Villa, “New developments on mini/micro shape memory actuators,” in *Smart Actuation and Sensing Systems: Recent Advances and Future Challenges* (IntechOpen, 2012).
<https://doi.org/10.5772/50473>
5. A. Rao, A. R. Srinivasa, and J. N. Reddy, *Design of Shape Memory Alloy (SMA) Actuators* (Springer, 2015).
6. A. Spaggiari, G. Sciré Mammano, and E. Dragoni, “Optimum mechanical design of binary actuators based on shape memory alloys,” in *Smart Actuation and Sensing Systems: Recent Advances and Future Challenges* (IntechOpen, 2012).
<https://doi.org/10.5772/50147>
7. K. Ootsuka, K. Shimizu, Yu. Suzuki, et al., *Shape Memory Alloys* (Metallurgiya, Moscow, 1990).
8. R. A. Abubakar, F. Wang, and L. Wang, “A review on nitinol shape memory alloy heat engines,” *Smart Mater. Str.* **30**, 013001 (2021).
9. M. Yu. Kollerov, D. E. Gusev, S. I. Gurtovoi, G. V. Gurtovaya, and A. V. Burnaev, “Laws of the shape recovery of titanium nickelide-based alloys under constant counteraction conditions,” *Titan*, No. 1, 38–43 (2014).
10. D. B. Chernov, “Principles of application of thermomechanical actuators in control systems,” *Inform.-Izm. Upravl. Sistemy* **14** (8), 36–42 (2016).
11. O. V. Letenkov and D. A. Filippov, “Calculation of a drive system: a spring made of a shape memory material—a counter spring,” *Mezhd. Nauch.-Issled. Zh.*, No. 11 (53), Part 4, 77–81 (2016).
<https://doi.org/10.18454/IRJ.2016.53.217>
12. T. Videnic, M. Brojan, J. Kunavar, and F. Kosel, “A simple one-dimensional model of constrained recovery in shape memory alloys,” *Mech. Adv. Mater. Str.* **21**, 376–383 (2014).
13. R. W. Wheeler, O. Benafan, F. T. Calkins, X. Gao, Z. Ghanbari, G. Hommer, D. Lagoudas, D. Martin, D. E. Nicholson, A. Petersen, F. R. Phillips, A. P. Stebner, and T. L. Turner, “Engineering design tools for shape memory alloy actuators: CASMART collaborative best practices and case studies,” *J. Intel. Mater. System. Str.* **30** (18–19), 2808–2830 (2019).
14. N. L. D. Sarmiento, J. M. Basílio, M. F. Cunha, C. R. Souto, and A. Ries, “Force control of a shape memory alloy spring actuator based on internal electric resistance feedback and artificial neural networks,” *Appl. Artificial Intel.* (2021).
<https://doi.org/10.1080/08839514.2021.2015106>
15. H. Stroud and D. Hartl, “Shape memory alloy torsional actuators: a review of applications, experimental investigations, modeling, and design,” *Smart Mater. Str.* **29**, 113001 (2020).
16. G. Shimoga, T.-H. Kim, and S.-Y. Kim, “An intermetallic NiTi-based shape memory coil spring for actuator technologies,” *Metals* **11**, 1212 (2021).
17. J. Koh, “Design of shape memory alloy coil spring actuator for improving performance in cyclic actuation,” *Materials* **11**, 2324 (2018).
18. O. Benafan, J. Brown, and F. T. Calkins, “Shape memory alloy actuator design: CASMART collaborative best practices and case studies,” *Int. J. Mech. Mater. Design.*, No. 10, 1–42 (2014).
19. M. Yu. Kollerov, D. E. Gusev, S. I. Gurtovoi, and A. V. Burnaev, “Thermomechanical behavior of titanium nickelide-based alloys at a constant counteraction,” *Russ. Metall. (Metally)*, No. 9, 808–814 (2018).
20. M. Yu. Kollerov, D. E. Gusev, A. V. Burnaev, and A. A. Sharonov, “Effect of the chemical composition and structure on the thermomechanical behavior of alloys based on titanium nickelide,” *Met. Sci. Heat Treat.* **59** (5, 6), 363–369 (2017).
21. D. E. Gusev, M. Yu. Kollerov, and R. E. Vinogradov, “Effect of a structure and test conditions on the critical strains and stresses in titanium nickelide-based alloys,” *Russ. Metall. (Metally)*, No. 4, 309–314 (2019).
22. M. Yu. Kollerov, D. E. Gusev, M. B. Afonina, and R. E. Vinogradov, “Effect of structure on the critical stresses and strains in titanium nickelide-based alloys,” *Russ. Metall. (Metally)*, No. 7, 760–766 (2020).
23. K. Otsuka and X. Ren, “Physical metallurgy of Ti–Ni-based shape memory alloys,” *Progr. Mater. Sci.*, No. 5 (50), 511–678 (2005).
24. *ASTM F2082/F2082M-2016. Standard Test Method for Determination of Transformation Temperature of Nickel–Titanium Shape Memory Alloys by Bend and Free Recovery* (ASTM International, West Conshohocken, 2016).
25. A. Stebner, S. Padula, R. Noebe, B. Lerch, and D. Quinn, “Development, characterization, and design considerations of Ni₁₉.5Ti₅₀.5Pd₂₅Pt₅ high-temperature shape memory alloy helical actuators,” *J. Intel. Mater. System. Str.* **20** (17), 2107–2126 (2009).

Translated by K. Shakhlevich